Pergamon

Bioorganic & Medicinal Chemistry 10 (2002) 1919–1927

BIOORGANIC & MEDICINAL CHEMISTRY

Photo-Control of Nitric Oxide Synthase Activity Using a Caged Isoform Specific Inhibitor

Heather J. Montgomery,[a,†] Basil Perdicakis,[b,†] Dan Fishlock,[a,†] Gilles A. Lajoie,[a] Eric Jervis[b] and J. Guy Guillemette[a,*]

[a]*Department of Chemistry, University of Waterloo, Waterloo, Ontario, Canada N2L 3G1*
[b]*Department of Chemical Engineering, University of Waterloo, Waterloo, Ontario, Canada N2L 3G1*

Received 9 October 2001; accepted 18 December 2001

Abstract—Nitric oxide (NO) plays a critical role in a number of physiological processes and is produced in mammalian cells by nitric oxide synthase (NOS) isozymes. Because of the diverse functions of NO, pharmaceutical interventions which seek to abrogate adverse effects of excess NOS activity must not interfere with the normal regulation of NO levels in the body. A method has been developed for the control of NOS enzyme activity using the localized photochemical release of a caged isoform-specific NOS inhibitor. The caged form of an iNOS inhibitor has been synthesized and tested for photosensitivity and potency. UV and multiphoton uncaging were verified using a hemoglobin-based assay. IC_{50} values were determined for the inhibitor (70 ± 11 nM), the caged inhibitor (1098 ± 172 nM), the UV uncaged inhibitor (67 ± 26 nM) and the multiphoton uncaged inhibitor (73 ± 11 nM). UV irradiation of the caged inhibitor resulted in a 86% reduction in iNOS activity after 5 min. Multiphoton uncaging had an apparent first order time constant of 0.007 ± 0.001 min^{-1}. A therapeutic range exists, with molar excess of inhibitor to enzyme from 3- to 7-fold, over which the full dynamic range of the inhibition can be exploited.

Introduction

Nitric oxide is an inorganic free radical gas that is implicated in a number of biological functions. NO plays a crucial regulatory role in the cardiovascular system[1] and is involved in neurotransmission, non-specific immunity, vasodilation, platelet inhibition, bronchodilation, and contractions of heart and skeletal muscle, as well as perpetuating the inflammatory process upon tissue injury.[2] NO is produced in different mammalian tissues by three distinct nitric oxide synthase isoforms (NOS; EC 1.14.13.39). These enzymes are homodimeric proteins that catalyse a five-electron oxidation of L-arginine to yield NO and L-citrulline.

Two of the three NOS isoforms, endothelial (eNOS) and neuronal (nNOS), are constitutively expressed (cNOS) enzymes. The cNOS enzymes are inactive at basal cellular levels of calcium (Ca^{2+}). An influx of Ca^{2+} is necessary for calmodulin (CaM) to bind and activate these two NOS isozymes. The eNOS enzyme is membrane bound and is located in the endothelial lining of the vascular system.[3] The NO produced by eNOS diffuses into the smooth muscle cells lining the cardiovascular system causing relaxation. eNOS also inhibits the adhesion of leukocytes to the arterial and venous walls. The nNOS enzyme is active in the central and peripheral nervous system and produces NO that may be involved in neurotransmission and memory formation.[2] The unregulated Ca^{2+} influx occurring in cerebral ischemia causes nNOS to overproduce cytotoxic levels of NO.[4]

The transcriptionally regulated third isoform, inducible NOS (iNOS), was first identified in macrophages but is now recognized to be produced by most eukaryotic cells.[5] The production of iNOS is absent until induced by hypoxia/ischemia or immunostimulants such as bacterial lipopolysaccharide and cytokines.[2] Once expressed, iNOS is active, essentially unregulated, and produces NO at potentially cytotoxic levels, resulting in local tissue damage.[6] The control of NO production is therefore important in the regulation of a large number of physiological processes. During cerebral ischemia the role of NO is protective or destructive depending on the stage of evolution of the ischemic process and the cellular compartment producing NO.[7] In the acute phase of pathogenesis during ischemia, parenchymal and microvascular NO overproduction is due to activation of nNOS and eNOS. The NO produced by eNOS is likely beneficial by acting as a vasodilator and improving blood flow to the affected area by inhibiting platelet aggregation and

*Corresponding author. Tel.: +1-519-888-4567 x5954; fax: +1-519-746-0435; e-mail: jguillem@sciborg.uwaterloo.ca (J. G. Guillemette).
†These authors made equal contributions to the research.

0968-0896/02/$ - see front matter
PII: S0968-0896(02)00050-0

leukocyte adhesion.[8] In contrast, studies using nNOS knockout mice and selective inhibitors for nNOS indicate that NO produced by nNOS contributes to the initial metabolic deterioration of the infarct penumbra.[9–11]

NO produced by iNOS contributes to progressive tissue damage leading to larger infarcts during the later stages of the ischemic process.[12] Thus, the development of methods for the proper management of the spatial and temporal production of NO in the post-ischemic brain or heart may ultimately lead to treatments that will decrease cell damage from stroke and other pathophysiological processes associated with NO over-production. In addition, the controlled release of NOS isoform-specific inhibitors should allow for a more robust treatment program. The spatial and temporal control of inhibition would prevent undesirable side effects arising from inhibition of NO production by all three isoforms in other parts of the patient, (i.e., evidence of constitutive iNOS expression in the human retina, cerebellum, and skeletal muscle tissue has been reported).[13] To date there are no reported treatments that would permit selective inhibition of specific NOS isoforms with spatial and temporal control.

Multiphoton (MP) microscopy has recently been introduced as an alternative to standard confocal microscopy methods.[14,15] With MP excitation, molecular fluorescence is induced by absorbing two or more infrared (IR) photons simultaneously. MP excitation is achieved with femtosecond pulsed IR laser irradiation. The requirement of near simultaneous interaction of multiple photons with the target fluorophore produces a restricted region of fluorescence excitation about the focal volume (i.e., sufficient photon flux density only occurs at the focal point of the objective lens). For therapeutic purposes, MP absorption confers the advantages of intrinsic confinement of excitation, greater tissue penetration depth, and reduced tissue damage over visible and UV radiation sources.

MP techniques have been employed for the release of 'caged' compounds in biological samples.[16,17] Less than 1 μm^3 of sample is uncaged during irradiation because uncaging occurs only in the focal volume, thus permitting the spatially confined release of a molecule from a MP-labile protecting group. There is considerable ongoing research directed toward developing molecules with increased two-photon cross section.[18,19] Of particular significance to this report is the recent synthesis of 7-hydroxycoumarin-4-ylmethyl esters and carbamates with uncaging cross sections 100 times higher than previously reported for MP-induced uncaging.[20]

Here, we report the protection of the iNOS selective inhibitor 1400W[21] (**1**) with the MP-labile coumarin-derived protecting group developed by Furuta and co-workers[20] to produce the caged inhibitor (**3**) (Fig. 1). 1400W binds to human iNOS competitively with L-arginine, resulting in a time-dependent loss of enzyme activity.[21]

To our knowledge, this is the first reported conjugation of a caging molecule with a large two photon uncaging cross section to a therapeutic agent. This technology could be used to minimise NO related damage inflicted during ischemia or inflammation by selectively inhibiting NO production in the vicinity of affected tissues, while not interfering with iNOS activity in other regions of the body. The use of MP photolysis to selectively activate pharmaceuticals confers significant advantages over current therapies including minimisation of drug side effects in non-target tissue, real time control of drug concentration, and the delivery of active drugs to specific regions of tissue. Our current research is aimed at the creation of a new class of therapy where MP techniques are utilised in conjunction with caged therapeutics to effect spatial and temporal control of drug activation.

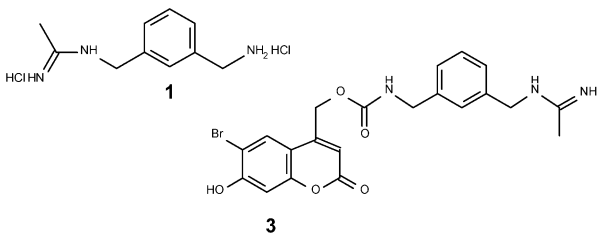

Figure 1. Molecular structures of 1400W (**1**) and Bhc-1400W (**3**).

Results

Properties of the inhibitor 1400W

The NOS inhibitor 1400W (**1**), was readily synthesised as previously described.[22] The amount of inhibition by 1400W was determined using a modified hemoglobin capture assay for the NOS enzyme.[23,24] An IC_{50} value of 70 ± 11 nM was measured for 1400W inhibition of the human iNOS enzyme. The human iNOS enzyme used in the investigation carries a deletion of the first 70 amino acids and an amino terminal polyhistidine tail.

While some NOS inhibitors covalently interact with the heme iron, others only bind near the heme iron. The type of substrate or inhibitor interaction can be monitored by optical difference spectroscopy.[25] Substrate perturbation spectroscopy was used to investigate the interactions of iNOS with L-arginine and 1400W. Increasing concentrations of 1400W added to iNOS cause a type-I difference spectrum similar to that obtained with L-arginine (results not shown). This is consistent with the recently published crystal structure of the eNOS–1400W complex.[26] The amidine group of 1400W was found to anchor the compound in the heme active site through hydrogen bonds to Glu 363 and the Trp 358 carbonyl oxygen.[26] Our K_s values for L-arginine and 1400W are 2.6 and 4.2 μM, respectively, in close agreement with reported kinetic constants for L-arginine ($K_s = 2.5$ μM)[25] and 1400W ($K_I = 2.0$ μM).[21]

Properties of the caged inhibitor Bhc-1400W

Coupling of the 6-bromo-7-hydroxy-4-hydroxymethylcoumarin (Bhc) (**2**) group to 1400W via a carbamate

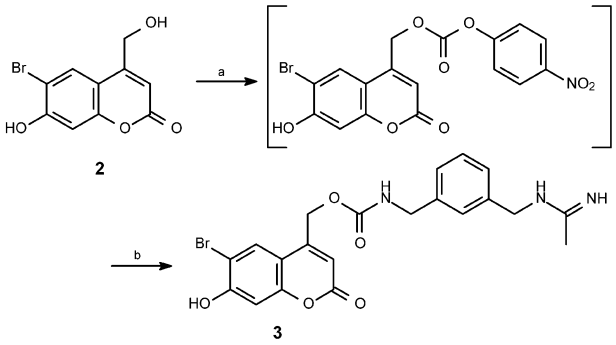

Scheme 1. (a) DMAP, 4-nitrophenylchloroformate, CH_3CN, rt, 9 h; (b) **1**, DMAP, 24 h.

linker produced the caged compound Bhc-1400W (**3**) (Scheme 1).

Although Bhc-1400W was readily soluble in 10% methanol, ethanol, or DMSO, the presence of these solutions was found to interfere with enzyme kinetics. Further investigation determined that Bhc-1400W was soluble in KMops buffer (pH 7.2) with a maximum solubility of approximately 900 μM. Stock solutions in KMops at 600 μM were routinely prepared. No dark uncaging was observed for a 300 μM sample after 6.5 h storage at 4° in the dark (Fig. 2).

The type of inhibitor interaction, if any, occurring between Bhc-1400W and the heme iron of NOS could not be determined using the substrate perturbation spectroscopy method described for 1400W due to the strong absorbance maximum of coumarin at 370 nm. Although the coumarin is coupled via the amine of 1400W so that the amidine remains free to associate with the guanidine-binding pocket of the enzyme, it is unknown whether Bhc-1400W still binds in the vicinity of the heme prior to electron transfer.

Photolysis of Bhc-1400W

The uncaging kinetics of Bhc-1400W by one-photon excitation was determined by irradiating Bhc-1400W with 366 nm UV light for given time periods. Fluorescence excitation at 340 nm and emission detection at 465 nm revealed that coumarin photo-bleaching was complete in less than 15 min (data not shown). The release of 1400W was characterized by apparent first order kinetics with a time constant of 0.39 ± 0.28 min^{-1} ($R^2 = 0.95$). UV irradiation of Bhc-1400W resulted in a 86% reduction in iNOS activity after 5 min (Fig. 2). TLC and ESI-MS were also used to monitor the uncaging of Bhc-1400W. NMR studies on the purified coumarin by-product revealed the coumarin ring to be intact.

MP uncaging of Bhc-1400W was performed at 740 nm[20] and the laser power exiting the cuvette was approximately 350 mW. MP irradiation of Bhc-1400W resulted in a 60% reduction in iNOS activity after 80 min (Fig. 2). MP uncaging data was fit to a decaying exponential yielding an apparent first order rate constant of 0.007 ± 0.001 min^{-1}. The uncaging of Bhc-1400W by

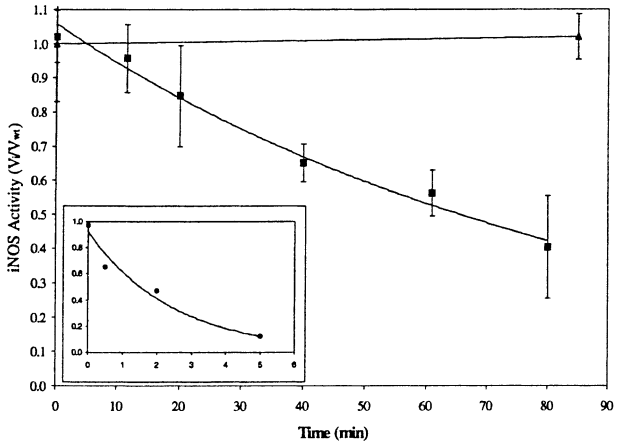

Figure 2. Time course of photolysis of Bhc-1400W. The kinetics of photolysis following ultra-violet (●, inset) or two-photon IR (■) irradiation compared to uncaging in the dark (▲). Fractional conversion of Bhc-1400W to 1400W versus uncaging time data was fit to a decaying exponential with a time constant of 0.007 ± 0.001 min^{-1} for two-photon IR uncaging ($R^2 = 0.98$) and 0.39 ± 0.28 min^{-1} for UV uncaging ($R^2 = 0.95$). Error bars indicate 95% confidence intervals and are representative of collected data.

MP showed similar kinetics to that of Bhc-glutamate as determined by Furuta and co-workers (first order rate constant of 0.026 min^{-1}).[20] Discrepancies between the estimated rate constants are likely due to the higher power (530 mW exiting the cuvette) and different optics utilised by Furuta et al.[20] Exposure of Bhc-1400W to a non-mode-locked infrared beam exiting the Ti/Sapphire laser for 1 h did not result in fluorescence or uncaging, verifying that the multiphoton effect is required to photoactivate Bhc-1400W. The in vitro enzyme assay was used to ensure that MP photolysis of Bhc-1400W produced the desired biological effect.

IC_{50} values of 1400W and Bhc-1400W

IC_{50} curves were obtained by normalising the initial enzymatic rates of inhibitor titrations with the uninhibited enzyme's initial rate. All analyses were carried out in quadruplicate in 96-well plates. To simplify the comparison of regression results, the maximal and minimal reaction rates were normalized to 1 and 0, respectively, to reduce the four-parameter to the two-parameter logistic eq 1. This simplification did not significantly affect the calculated parameters and resulted in a good fit to experimental data (Fig. 3). Results for 1400W, Bhc-1400W, UV uncaged 1400W, and MP uncaged 1400W were fit by nonlinear regression (Statistics Toolbox, MATLAB version 5.3, Mathworks, Boston, MA) to eq 1:

$$\frac{V_I}{V_{WT}} = \frac{1}{1 + \left(\frac{[I]}{IC_{50}}\right)^n} \quad (1)$$

where V_I is the initial rate of L-arginine consumption at inhibitor concentration I (nM L-arginine min^{-1} mg^{-1} enzyme), V_{WT} is the initial rate of L-arginine consumption for inhibitor-free reactions (nM L-arginine min^{-1}

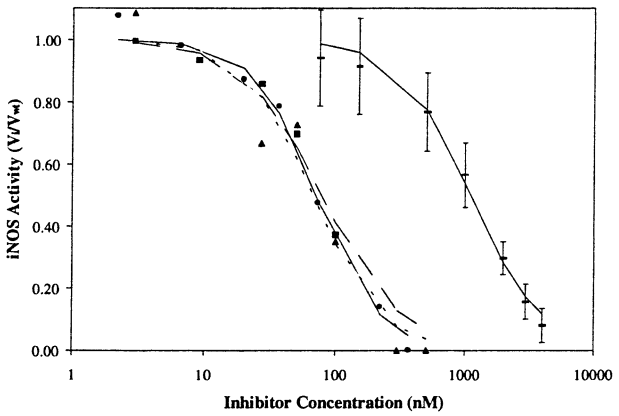

Figure 3. IC_{50} curves of 1400W, Bhc-1400W, MP uncaged Bhc-1400W, and UV uncaged Bhc-1400W. The IC_{50} values for 1400W (●, 70 nM), Bhc-1400W (-, – 1098 nM), MP uncaged Bhc-1400W (■, – –, 73 nM), and UV uncaged Bhc-1400W (▲,---, 67 nM) were determined. Samples were pre-incubated for 15 min at 30 °C in the presence of 500 μM NADPH, 287 nM iNOS and varying concentrations of inhibitor. Reactions were initiated by the addition of 10 μM L-arginine. Error bars indicate 95% confidence intervals and are representative of collected data.

mg^{-1} enzyme), [*I*] is the inhibitor concentration (nM), and *n* is the logistic sensitivity (Hill coefficient) (Table 1).

The IC_{50}/[E] values, following 15 min of enzyme-inhibitor pre-incubation, for 1400W were 22 and 382 times greater for nNOS and eNOS, respectively, when compared to iNOS. The caging of 1400W with Bhc produced a compound with significantly reduced potency. The caged Bhc-1400W inhibited 50% of iNOS activity at a concentration of 1.1 ± 0.2 μM (Table 1)—15.7 times the amount of 1400W required to obtain the same degree of inhibition. Coupling of the Bhc molecule did not affect isoform selectivity of 1400W as no nNOS or eNOS inhibition by Bhc-1400W was observed (Table 1). Uncaging of Bhc-1400W by either MP (150 min) or UV (5 min) irradiation quantitatively released 1400W with iNOS IC_{50} values of 73 ± 11 and 67 ± 26 nM, respectively. There was no statistically significant variation in the calculated Hill coefficients.

The calculated IC_{50} values for 1400W and the UV and MP uncaged Bhc-1400W are in excellent agreement, indicating that fully uncaged samples possess the same potency for iNOS as native 1400W. Due to the limited solubility of Bhc-1400W ($\leq$900 μM), IC_{50}/[E] values could not be obtained for the nNOS and eNOS enzymes. Nonetheless the UV and MP uncaged Bhc-1400W also maintained the iNOS isoform specificity of 1400W. The large ratio of the 1400W IC_{50} to the Bhc-1400W IC_{50} value demonstrates the therapeutic potential of this caged inhibitor. For example, Figure 3 indicates that a Bhc-1400W dose of 200 nM results in a 7% reduction of iNOS activity, while MP uncaging of this sample results in an 89% reduction of iNOS activity.

Time-dependent inhibition of iNOS by 1400W and Bhc-1400W

1400W is a slow tight-binding inhibitor of iNOS.[21] Time dependent inhibition occurs when the attainment of equilibrium between enzyme and inhibitor is slow relative to the rate of enzymatic turnover.[27] Two potential mechanisms for time-dependent inhibition are:[28]

$$E + I \underset{k_4}{\overset{k_3}{\rightleftharpoons}} EI \tag{A}$$

$$E + I \underset{k_4}{\overset{k_3}{\rightleftharpoons}} EI \underset{k_6}{\overset{k_5}{\rightleftharpoons}} EI^* \tag{B}$$

In mechanism A, the time dependence of inhibition is a result of the slow formation of the EI complex, whereas in mechanism B it is due to the slow rate of a secondary conformational change of the EI complex to an EI* complex. Equilibrium concentrations of enzyme, inhibitor, and the EI complex are related by the dissociation constant, which is defined as:[27]

$$K_i = \frac{[E][I]}{[EI]} \tag{2}$$

For mechanism B the overall dissociation constant for a slow binding inhibitor is:

$$K_i^* = K_i \frac{k_6}{k_5 + k_6} \tag{3}$$

1400W is a competitive inhibitor of iNOS, and in the presence of L-arginine, K_i is related to an apparent K_i by:

$$K_i^{app} = K_i \left(1 + \frac{[S]}{K_M}\right) \tag{4}$$

Table 1. Inhibition kinetics of iNOS, nNOS and eNOS by 1400W, Bhc-1400W and uncaged Bhc-1400W

Inhibitor	iNOS		nNOS		eNOS	
	IC_{50}/[E]	*n*	IC_{50}/[E]	*n*	IC_{50}/[E]	*n*
1400W	2.4 ± 0.4	1.8 ± 0.6	53 ± 9	1.8 ± 0.6	916 ± 170	1.3 ± 0.3
Bhc-1400W	38 ± 6	1.6 ± 0.3	NAI		NAI	
UV uncaged Bhc-1400W	2.3 ± 0.9	1.6 ± 1.0	NCIS		NAI	
MP uncaged Bhc-1400W	2.6 ± 0.4	2.1 ± 0.7	NCIS		NAI	

Enzyme concentrations were 28.7 nM for iNOS and nNOS, and 1170 nM for eNOS.
NAI, no apparent inhibition.
NCIS, no change in isoform specificity.
95% Confidence intervals are shown.
n, logistic sensitivity (Hill coefficient) from eq 1.

Time-dependent inhibition of iNOS by free and caged inhibitor was studied by the addition of iNOS to reaction solutions containing L-arginine and 1400W or Bhc-1400W. The resulting progress curve data was fit to eq 5 by nonlinear regression analysis:[28,29]

$$A_{401}(t) - A_{401}(t=0) = \nu_s t + \frac{(\nu_0 - \nu_s)(1 - \exp(-k_{obs}t))}{k_{obs}} \quad (5)$$

where $A_{401}(t)$ is the absorbance at 401 nm at time t (OD), ν_0 is the initial velocity (OD/s), ν_s is the steady state velocity (OD/s), and k_{obs} is the apparent first order rate constant for the conversion of ν_0 to ν_s (s^{-1}).[28] Figure 4A shows typical progress curves generated in the presence of 1400W and Bhc-1400W. Experimental data were fit to eq 5 while the uninhibited control reaction was linear. For all experiments the inhibitor concentration was appreciably greater than the total enzyme concentration.[28] iNOS, L-arginine, and oxyhemoglobin concentrations of 10 nM, 20 μM, and 15 μM, respectively, were selected to allow sufficient time to observe the curvilinear nature of the inhibited progress curves and maintain a linear OD versus methemoglobin production relation with an adequate signal to noise ratio.

The inhibition kinetics of 1400W conformed to mechanism B, agreeing with the results of Garvey and co-workers,[21] and fit to the following rectangular hyperbolic relation:[28,29]

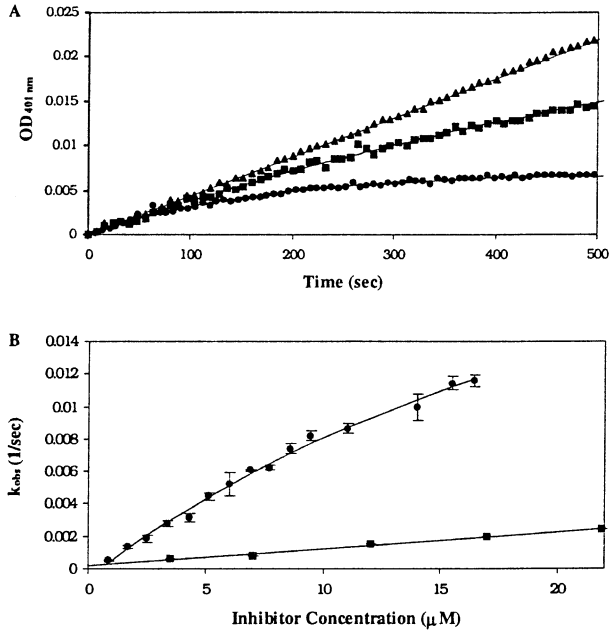

Figure 4. Inhibition kinetics of iNOS with 1400W and Bhc-1400W. Panel A, iNOS activity for representative 1400W (●, $k_{obs} = 6.0\times10^{-3}$ s^{-1}) and Bhc-1400W (■, $k_{obs} = 1.4\times10^{-3}$ s^{-1}) at concentrations of 6 μM and 12 μM, respectively. Inhibitor-free iNOS activity (▲) is also shown. Panel B, k_{obs} versus 1400W (●, $k_5 = 0.035$ s^{-1}, $k_6 < 1.9\times10^{-6}$ s^{-1}, $K_i = 9.3$ μM, maximum $K_i^* = 508$ pM) and Bhc-1400W (■, $k_{on}^{app} = 3.3\times10^{-4}$ μM^{-1} s^{-1}, $k_6 = 2.1\times10^{-4}$ s^{-1}) concentrations. Error bars indicate ±1 standard deviation.

$$k_{obs} = k_6 + \left(\frac{k_5[I]}{K_i^{app} + [I]}\right) \quad (6)$$

The k_{obs} versus inhibitor concentration data for 1400W and Bhc-1400W are shown in Figure 4B. For 1400W, values of K_i^{app} of 30±7.3 μM, k_5 of (3.5±0.5)×10^{-2} s^{-1}, and a maximum k_6 value of 1.9×10^{-6} s^{-1} characterizing slow tight binding inhibition of iNOS were obtained by nonlinear regression of eq 6 to the 1400W data (Fig. 4B). Accurate k_{obs} values could not be obtained at higher 1400W concentrations due to rapid inhibition kinetics. This problem has previously been encountered by others.[21] Substituting a K_i^{app} of 30±7.3 μM, a [S] of 20 μM, and a K_M of 9±0.8 μM into eq 4 results in a K_i of 9.3±2.4 μM for 1400W. Substituting a K_i of 9.3±2.4 μM, a $k_{6\ max}$ of 1.9±10^{-6} s^{-1}, and a k_5 of (3.5±0.5) ×10^{-2} s^{-1} into eq 3 results in a $K_i^*{}_{max}$ of 508±152 pM for 1400W. The kinetic parameters calculated characterizing the slow tight binding inhibition of iNOS by 1400W are in good agreement with the values of 2±0.5 μM for K_i, 0.028±0.003 s^{-1} for k_5, and (7.3±0.6)×10^{-5} s^{-1} for k_{6max} reported by Garvey and co-workers.[21]

Bhc-1400W is a slow binding inhibitor of iNOS when examined under the given experimental conditions; the Bhc-1400W IC_{50} value, after 15 min of pre-incubation with iNOS, is one order of magnitude greater than the total iNOS concentration.[27] Thus the coumarin moiety substantially reduces the tight binding of 1400W to iNOS. The linear k_{obs} versus Bhc-1400W relation shown in Figure 4B is likely due to the degeneration of eq 6 into a linear relation when $[I] << K_i^{app}$ as indicated by eqs 7 and 8:

$$k_{obs} = k_6 + \left(\frac{k_5[I]}{K_i^{app}}\right) = k_6 + k_{on}^{app}[I] \quad (7)$$

$$k_{on} = k_{on}^{app}\left(1 + \frac{[S]}{K_M}\right) = \frac{k_5}{K_i} \quad (8)$$

where k_{on}^{app} (μM^{-1} s^{-1}) is the slope of the k_{obs} versus [I] plot. An alternate, but unlikely, explanation for the linear k_{obs} versus [Bhc-1400W] relation is that coupling of the Bhc moiety to 1400W alters the mode of inhibition from mechanism B to A. For Bhc-1400W, a k_6 value of (2.1±0.7)×10^{-4} s^{-1} and a k_{on} value of (3.3±0.3)×10^{-4} s^{-1} characterizes the slow binding inhibition of iNOS as obtained by linear regression of the Bhc-1400W data (Fig. 4B).

PC12 cell viability in the presence of 1400W and Bhc-1400W

The viability of PC12 cells incubated with 1400W, Bhc-1400W and 7-amino-4-methly-coumarin for 48 h was determined by exclusion of erythrosine B dye. The highly soluble 1400W was toxic at concentrations above 5 mM and gave an ED_{50} value of 1 mM. In the presence

of 1 mM Bhc-1400W the viability of the PC12 cells was 39%. Lowering the concentration of Bhc-1400W 10-fold to 100 μM increased the viability of the PC12 cells to 80%. Only a low concentration of 7-amino-4-methly-coumarin (27 μM) was soluble in the 25 mM HEPES/McCoy's media used. This concentration of 7-amino-4-methly-coumarin was non-toxic to PC12 cells.

Discussion

N-(3-(Aminomethyl)benzyl)acetamidine (1400W) was selected for investigation because it has the highest reported potency and selectivity for iNOS inhibition.[21] The inhibition of eNOS and nNOS by 1400W is rapidly reversible and inefficient. The extremely slow off-rate of 1400W bound to iNOS makes it a potent inhibitor. The caging of 1400W did not affect isoform selectivity. A large decrease in the level of iNOS inhibition by the caged compound yields a wide therapeutic range over which the full action of the inhibitor can be exploited. The poor inhibitory properties of Bhc-1400W are likely due to the loss of a positive charge and steric effects by conversion of the amine to a carbamate.

Coupling Bhc to 1400W may significantly increase the off-rate (k_6) of the inhibitor when bound to iNOS, resulting in a substantial reduction in potency. This is consistent with the observation that the Bhc-1400W and 1400W show poor inhibition of the constitutive NOS isoforms. The calculated k_6 value for Bhc-1400W is approximately 100-fold greater than that of the maximum 1400W value. The K_i value for Bhc-1400W is also substantially larger than that of 1400W, as no curvature for the Bhc-1400W data is apparent in Figure 4B. The reduction in potency of iNOS inhibition by Bhc-1400W, as compared to 1400W, is a result of higher k_6 and K_i values and a reduced k_5 value. These effects would substantially increase the overall slow binding inhibitor dissociation constant (K_i*) for Bhc-1400W. This result is supported by the 15-fold increase in the IC_{50} value of Bhc-1400W compared to 1400W as shown in Table 1.

MP irradiation has been recently employed for the release of caged compounds in biological samples.[8,19,30] The spatially confined release of caged molecules is possible because uncaging occurs only in the focal volume—less than 1 μm^3 of sample. With IR irradiation, molecules can be uncaged without tissue damage at significantly greater depths than possible with UV irradiation.

Over the past decade MP microscopy has progressed from a novel technology to an important tool in medical research. Neural imaging of freely moving rats by means of a head mounted MP microscope and a single-mode optical fiber has recently been demonstrated.[31] A similar device could be utilized to investigate photoactivation of a caged therapeutic in the cortex following surgically induced focal ischemia. Continued advancements in MP microscopy will enable researchers to explore the use of this technology in an increasing number of therapeutic applications.

This report provides the first example of a caged NOS inhibitor that undergoes multiphoton photoactivation. A similar approach can be used for a variety of applications including photodynamic therapies and non-invasive mapping of cellular responses to uncaged molecules. The synthesis of a drug covalently bound to a fluorophore with a large two-photon cross section is a novel class of compounds with the potential to be photoactivated allowing for the spatial and temporal control of drug activity in tissue. This approach should greatly expand the available range of therapeutics that may otherwise not be used because of side effects in non-target tissues.

Experimental

Materials

All reagents were purchased from Sigma-Aldrich Canada, Ltd. (Oakville, ON, Canada) and used without further purification. Electrospray ionization-mass spectrometry (ESI-MS) was performed in positive ion mode on a Micromass Quattro II triple quadrupole mass spectrometer equipped with an electrospray source (Micromass, Manchester, UK). Samples were introduced by flow injection analysis using acetonitrile/water (1:1) with 0.1% formic acid as solvent. Cone voltage was set to 10 V for all samples. High-resolution mass spectrometry was performed using a Quadrupole Time-Of-Flight (QTOF) (Micromass, Manchester, UK) using an appropriate internal standard.

Synthesis of the free and caged forms of 1400W

N-(3-(Aminomethyl)benzyl)acetamidine dihydrochloride (1400W) 1.[22] A solution of *m*-xylyenediamine (5 g, 36.71 mmol) and triethylamine (2.55 g, 18.34 mmol) in dry methanol (100 mL) was cooled to 0 °C. To this solution, di-*t*-butyldicarbonate (4 g, 18.34 mmol) in THF (30 mL) was added drop-wise over 1 h. The reaction was stirred an additional 2 h at 0 °C under argon, and then filtered. The filtrate was concentrated, then purified by silica column chromatography by elution with 5:95:0.5 $MeOH/CH_2Cl_2/NH_4OH$. *t*-Butyl-*N*-(3-(aminomethyl)benzyl) carbamate (2.44 g, 28% yield) was obtained as a viscous yellow oil. *t*-Butyl-*N*-(3-(aminomethyl)benzyl) carbamate (2 g, 8.4 mmol) was dissolved in ethanol (25 mL) at 0 °C under argon. *S*-2-Naphthylmethyl thioacetimidate hydrobromide[32] (2.5 g, 8.4 mmol) was added, and the cloudy mixture was stirred for 4 h as it warmed to room temperature. The mixture was concentrated in vacuo and the resultant off-white solid was taken up in 1:1 H_2O/Et_2O (150 mL), and washed three times with Et_2O (50 mL). The aqueous fraction was lyophilized to provide *t*-butyl-*N*-(3-((acetamidoyl)-aminomethyl)benzyl carbamate hydrobromide (*N*-BOC-1400W) (1.97 g, 65% yield) as a white waxy solid. *N*-BOC-1400W (1 g, 2.8 mmol) was dissolved in anhydrous dioxane (20 mL) and 4 N HCl in dioxane (5 mL) under argon and stirred for 24 h at room temperature. The reaction mixture was diluted with Et_2O (30 mL) and the product collected by

filtration and dried under vacuum with gentle heating to yield **1** as off-white flakes (0.68 g, 96% yield). ^{1}H NMR (300 MHz, D_2O) δ 7.27–7.40 (4H, m), 4.4 (2H, s), 4.06 (2H, s), 2.15 (3H, s); ^{13}C NMR (75 MHz, D_2O) δ 165.0, 135.2, 133.4, 129.9, 128.7, 128.4, 127.9, 45.5, 42.9, 18.5. ES-MS (MH^+) 177.9.

6 - Bromo - 7 - hydroxy - 4 - hydroxymethylcoumarin 2.[20] 4-Bromoresorcinol (922.5 mg, 4.881 mmol) was stirred in concentrated H_2SO_4 (5 mL) with ethyl 4-chloroacetoacetate (1 mL, 7.4 mmol) for 6 days at room temperature. This mixture was poured into 50 mL of ice cold H_2O and stirred vigorously for 2 h. The precipitate was filtered, washed with ice-cold H_2O, and dried over P_2O_5, to provide the brown, granular 6-bromo-7-hydroxy-4-chloromethyl-coumarin (0.547 g, 39% yield). This chloride (450 mg, 1.55 mmol) was suspended in 75 mL H_2O and refluxed for 4 days, then lyophilized to provide **6** as a brown powder (370 mg, 88% yield). ^{1}H NMR (250 MHz, CD_3OD) δ 7.80 (1H, s), 6.83 (1H, s), 6.37 (1H, s), 4.76 (2H, s); ^{13}C NMR (75 MHz, $(CD_3)_2CO$) δ 160.1, 156.9, 155.1, 154.4, 128.2, 111.9, 108.6, 105.8, 103.4, 59.7. ES-MS (MH^+) 270.7, 272.7 (1:1).

***N*-(6-Bromo-7-hydroxycoumarin-4-yl)methoxy-carbonyl-*N*-(3-(aminomethyl)benzyl)acetamidine (Bhc-1400W) 3.** **2** was suspended in dry acetonitrile (20 mL), to which was added 4-nitrophenylchloroformate (111 mg, 1.2 mol equiv) and DMAP (112 mg, 2 mol equiv). This was stirred for 9 h under argon, after which time a solution of **1** (114 mg, 0.99 mol equiv) and DMAP (112 mg, 2 mol equiv) in DMF (10 mL) was added. After 24 h of stirring under argon in the dark, the reaction mixture was concentrated in vacuo to a dark yellow oil. This was suspended in 1:1 $CHCl_3/H_2O$ (50 mL), and washed three times with $CHCl_3$ (25 mL). The aqueous fraction (containing the product **3**) was lyophilized, then **3** was purified by silica chromatography eluting with 7:2.5:0.5 $CHCl_3$/MeOH/NH_4OH (R_f 0.23). The caged compound **3** (40 mg, 20% yield) was obtained as a pale-yellow powder. ^{1}H NMR (300 MHz, CD_3OD) δ 7.52 (1H, s), 7.17–7.47 (4H, m), 6.08 (1H, s), 5.63 (1H, s), 5.11 (2H, s), 4.38 (2H, s), 4.20 (2H, s), 2.16 (3H, s); ^{13}C NMR (75 MHz, CD_3OD) δ 170.9, 166.1, 165.0, 158.2, 157.4, 153.8 141.6, 136.0, 130.3, 128.4, 127.9, 127.6, 115.1, 106.6, 106.0, 104.0, 63.2, 47.3, 45.2, 18.4. ES-MS (MH^+) 473.78, 475.71 (1:1). HR-QTOF MH^+ ($C_{21}H_{20}BrN_3O_5$) expected 474.0665, found 474.0652. Fmoc-Tyr(O*t*Bu)(MH^+ 460.2124) used as internal standard.

Uncaging Bhc-1400W

Dried Bhc-1400W was dissolved in 250 to 1000 μL of 100 mM KCl/10 mM Mops buffer (pH 7.2) (KMops) by shaking the solution for 30 min at 4 °C in the dark. The concentration in solution was measured using UV–vis spectrophotometry ($\lambda_{max} = 368$ nm, $\varepsilon = 17{,}470\ M^{-1}\ cm^{-1}$).[20] UV light at 366 nm was used to uncage Bhc-1400W. Ten 10-μL aliquots were taken after various exposure times and the amount of uncaging in each sample was determined by the kinetic assay described below.

Multiphoton uncaging was performed by placing a micro-cuvette in the focal plane of an objective lens (Axoplan 10×/0.25 Ph 1) located at the exit aperture of a femtosecond mode-locked Ti/Sapphire laser (Mira Model 900-B laser, Coherent, Inc., Santa Clara, CA, USA) (76 MHz repetition rate, ≈200 fs pulse width). The Mira laser was pumped with 5 W at 532 nm (Coherent Verdi laser, Coherent, Inc., Santa Clara, CA, USA). Ten-μL aliquots of Bhc-1400W were used to obtain blank and multiphoton uncaged samples at various times. Uncaging was performed at 740 nm.[20] The laser power exiting the cuvette was 350 mW. Dark uncaging of Bhc-1400W was monitored with a sample wrapped in foil and kept at room temperature. The amount of uncaging that occurred in the samples was determined by the kinetic assay described below.

Protein expression and purification

Human iNOS enzyme carrying a deletion of the first 70 amino acids and an amino terminal polyhistidine tail was co-expressed with calmodulin in *Escherichia coli* and purified using metal chelating chromatography followed by 2′,5′-ADP column chromatography. The expression and protein purification of human eNOS and rat nNOS enzymes in *E. coli* was performed as previously reported.[33]

Enzyme kinetics

The activity of NOS was determined using the hemoglobin capture assay[23,24] that yields results consistent with the direct radioactive assay that monitors the formation of L-[^{3}H]-citrulline from L-[^{3}H]-arginine.[32] Quadruplicate reactions were initiated by the addition of L-arginine and monitored on a 96-well plate reader (Spectramax 190, Molecular Devices, Sunnyvale, CA, USA) at 30 °C. Nitric oxide-mediated oxidation of oxyhemoglobin was monitored at 401 nm ($\varepsilon = 0.1036$ OD/nanomol).[23] The concentration of Bhc-1400W in the wells, as well as for UV and MP uncaged samples, was 178 nM. For the determination of IC_{50} values, 100 μL reaction mixtures contained 50 mM Tris–HCl (pH 7.5), 500 μM NADPH, 5.0 μM H_4B, 1.0 μM CaM, 1.0 mM $CaCl_2$, 1.0 mM DTT, 1.0 μM FAD, 1.0 μM FMN, 100 units/mL superoxide dismutase (SOD), 50 units/mL catalase, 5.0 μM bovine oxyhemoglobin, 0.2 mg/mL bovine serum albumin, 10 μM L-arginine and 28.7 nM iNOS ($V_{max} = 376 \pm 105$ nM min^{-1} mg^{-1} iNOS, K_M (L-ARG $= 9 \pm 0.8$ μM), determined over a L-arginine concentration of 5–25 μM). Enzyme in the presence or absence of varying amounts of 1400W, Bhc-1400W, or uncaged Bhc-1400W, and in the presence of 500 μM NADPH, 10.0 μM FAD, 10.0 μM FMN, 50.0 μM H_4B, 10.0 mM DTT, 100 units/mL SOD and 50 units/mL catalase were incubated at 30 °C for 15 min.[21] For these experiments the Bhc-1400W was exposed to UV light for 5 min or to MP irradiation for 150 min to obtain the uncaged samples.

Kinetic parameters characterizing slow binding inhibition of iNOS by 1400W and Bhc-1400W were calculated from progress curve data obtained using the hemoglobin

assay.[34] Reaction conditions were similar to those given above except that 15 μM bovine oxyhemoglobin, 20 μM L-arginine and 10 nM NOS were used. Under these conditions inhibitor-free reactions were linear for approximately 10 min and did not exceed the linear range of the spectrophotometer. Blank well data was subtracted from progress curve data. Blank wells containing only 200 μM 1400W and iNOS produced similar values to wells containing no iNOS. The addition of Bhc-1400W did not significantly contribute to background signal at 401 nm at the concentrations tested. The removal of FMN, FAD, DTT, and H_4B from the reaction mixture did not reduce iNOS activity, and improved signal to noise ratios. Reactions were initiated by the addition of iNOS.

Optical difference spectroscopy

Optical spectra were recorded on a Cary 1 Bio UV–vis spectrophotometer (Varian Instruments, Sugar Land, TX, USA), with a Peltier 1×1 temperature control accessory (Varian Instruments, Sugar Land, TX, USA). Sample and reference cuvettes initially contained 750 μL of 50 mM Tris–HCl, pH 7.5, 10% glycerol, and 3 μM iNOS at 15 C. The base line spectrum was adjusted to zero. L-Arginine or 1400W were titrated into sample cuvettes, while buffer was used to adjust the volume of the reference cuvette. Difference spectra were recorded after each addition from 350 to 500 nm at 0.2-nm intervals using a 2-nm slit width.[25] Final volume changes were less than 2%. The *x*-intercept of double-reciprocal plots of the difference in the peak to trough absorbances versus the concentration of L-arginine or 1400W were used to determine the spectral binding constants (K_s).

Fluorescence spectroscopy

Fluorescence analysis of 1400W, Bhc-1400W and uncaged Bhc-1400W was performed on a Spex Fluorolog-22 spectrofluorometer (John Yvon Horiba Group, Edison, NJ, USA). An excitation maximum of 340 nm and an emission maximum of 465 nm were determined for Bhc-1400W. No fluorescence was observed for 1400W over these wavelengths. For the analysis of uncaging by UV light, 10-μL aliquots were taken every 15–20 min over a 180-min time period. Samples were diluted in deionised, double distilled, filtered water to a final concentration of 8.3 μM and their fluorescence measured.

Viability of PC12 cells in the presence of inhibitor

The rat pheochromocytoma cell line PC12 was purchased from American Type Culture Collection (CATCC) and maintained in McCoy's media supplemented with 10% heat-inactivated horse serum and 5% heat-inactivated bovine calf serum at 37 °C, in a humidified atmosphere of 5% CO_2. Cells were passaged every 3 days. The cells were harvested, triturated with a 18-gauge needle, concentrated to 5×10^5 cells/mL and then plated in 96-well cell culture chambers (VWR Canlab, Mississauga, ON, Canada) at a concentration of 1×10^5 cells/mL. In all studies, the medium was changed to 25 mM HEPES/supplemented McCoy's media before plating. The viability of the cells was ~90% as determined by exclusion of the dye erythrosine B. 1400W (500 to 5×10^{-5} mM), 7-amino-4-methly-coumarin (29 uM) and Bhc-1400W (1 to 1×10^{-9} mM) were taken up into buffered McCoy's media, filter sterilized and added to the cells in decreasing concentrations. Cells were incubated at 37 °C for 48 h. The viability of the cells in the presence of these compounds was determined as described above.

Acknowledgements

This research was supported by a grant from the Natural Sciences and Engineering Research Council of Canada and the Heart and Stroke Foundation. We would like to thank Dr. E. Meiering for the use of the spectrofluorometer, Dr. J. Lepock for use of the mammalian cell culture facilities, and Elizabeth Jones for technical assistance.

References and Notes

1. Moncada, S.; Higgs, A. *N. Engl. J. Med.* **1993**, *329*, 2002.
2. Kleinert, H.; Boissel, J. P.; Schwarz, P. M.; Forestmann, U. In *Nitric Oxide, Biology and Pathobiology*; Ignarro, L. J., Ed.; Academic: New York, 2000; p 105.
3. Dawson, T. D.; Dawson, V. L. *Methods Enzymol.* **1996**, *268*, 349.
4. Bredt, D. S.; Snyder, S. H. *Annu. Rev. Biochem.* **1994**, *63*, 175.
5. Marletta, M. A. *J. Biol. Chem.* **1993**, *268*, 12231.
6. Estrada, C.; Gomez, C.; Martin, C.; Moncada, S.; Gonzalez, C. *Biochem. Biophys. Res. Commun.* **1992**, *186*, 475.
7. Iadecola, C. *Trends Neurosci.* **1997**, *20*, 132.
8. Lutz, P. L.; Nilsson, G. E. *The Brain Without Oxygen*, 2nd ed.; Chapman and Hall: New York, 1997.
9. Zhang, Z. G.; Reif, D.; Macdonald, J.; Tang, W. X.; Kamp, D. K.; Gentile, R. J.; Shakespeare, W. C.; Murray, R. J.; Chopp, M. *J. Cereb. Blood Flow Metab.* **1996**, *16*, 599.
10. Huang, Z.; Huang, P. L.; Panahian, N.; Dalkara, T.; Fishman, M. C.; Moskowitz, M. A. *Science* **1994**, *265*, 1883.
11. Hara, H.; Huang, P. L.; Panahian, N.; Fishman, M. C.; Moskowitz, M. A. *J. Cereb. Blood Flow Metab.* **1996**, *16*, 605.
12. Iadecola, C.; Zhang, F. Y.; Casey, R.; Nagayama, M.; Ross, M. E. *J. Neurosci.* **1997**, *17*, 9157.
13. Park, C. S.; Park, R.; Krishna, G. *Life Sci.* **1996**, *59*, 219.
14. Denk, W.; Strickler, J. H.; Webb, W. *Science* **1990**, *248*, 73.
15. Williams, R. M.; Piston, D. W.; Webb, W. *FASEB J.* **1994**, *8*, 804.
16. Denk, W. *Proc. Natl. Acad. Sci. U.S.A.* **1994**, *91*, 6629.
17. Adams, S. R.; Lev-Ram, V.; Tsien, R. *Chem. Biol.* **1997**, *867*, 1256.
18. Reinhardt, B. A.; Brott, L. L.; Clarson, S. J.; Dillard, A. G.; Bhatt, J. C.; Kannan, R.; Yuan, L.; He, G. S.; Prasad, P. N. *Chem. Mater.* **1998**, *10*, 1863.
19. Albota, M.; Beljonne, D.; Bredas, J. L.; Ehrlich, J. E.; Fu, J. Y.; Heikal, A. A.; Hess, S. E.; Kogej, T.; Levin, M. D.; Marder, S. R.; McCord-Maughon, D.; Perry, J. W.; Rockel, H.; Rumi, M.; Subramaniam, G.; Webb, W. W.; Wu, X. L.; Xu, C. *Science* **1998**, *281*, 1653.

20. Furuta, T.; Wang, S. S.-H.; Dantzker, J. L.; Dore, T. M.; Bybee, W. J.; Callaway, E. M.; Denk, W.; Tsien, R. Y. *Proc. Natl. Acad. Sci. U.S.A.* **1999**, *96*, 1193.
21. Garvey, E. P.; Oplinger, J. A.; Furfine, E. S.; Kiff, R. J.; Laszio, F.; Whittle, B. J. R.; Knowles, R. G. *J. Biol. Chem.* **1997**, *272*, 4959.
22. Oplinger, J. A.; Garvey, E. P.; Furfine, E. S.; Shearer, B. G.; Collins, J. L. US Patent 5 866 612, 1999.
23. Gross, S. S. *Methods Enzymol.* **1996**, *267*, 159.
24. Hevel, J. M.; Marletta, M. A. *Methods Enzymol.* **1994**, *233*, 250.
25. McMillan, K.; Masters, B. S. S. *Biochemistry* **1993**, *32*, 9875.
26. Li, H.; Raman, C. S.; Martasek, P.; Masters, B. S. S.; Poulos, T. L. *Biochemistry* **2001**, *40*, 5399.
27. Copeland, R. A. *Enzymes: A Practical Introduction to Structure, Mechanism and Data Analysis*; Wiley-VCH: New York, 1996.
28. Morrison, J. F.; Walsh, C. T. *Adv. Enzymol. Relat. Areas Mol. Biol.* **1988**, *61*, 201.
29. Szedlacsek, S. E.; Duggleby, R. G. *Methods Enzymol.* **1995**, *249*, 144.
30. Brown, E. B.; Webb, W. *Methods Enzymol.* **1998**, *291*, 356.
31. Helmchen, F.; Fee, M. S.; Tank, D. W.; Denk, W. *Neuron* **2001**, *31*, 903.
32. Shearer, B. G.; Oplinger, J. A.; Lee, S. *Tetrahedron Lett.* **1997**, *38*, 179.
33. Montgomery, H. J.; Romanov, V.; Guillemette, J. G. *J. Biol. Chem.* **2000**, *275*, 5052.
34. Dawson, J.; Knowles, R. G. *Mol. Biotechnol* **1999**, *12*, 275.